

Photocatalytically Driven Dissolution of Macroscopic Nickel Surfaces

Richard J. Wilbraham[†], Colin Boxall^{†}, Robin J. Taylor[‡]*

The LRF Centre for Nuclear Engineering, Engineering Department, Lancaster University, Bailrigg,
Lancashire, LA1 4YR, United Kingdom and National Nuclear Laboratory, Central Laboratory,
Seascale, Cumbria, CA20 1PG, United Kingdom

r.wilbraham@lancaster.ac.uk, c.boxall@lancaster.ac.uk, robin.j.taylor@npl.co.uk

RECEIVED DATE

*To whom all correspondence should be sent. E-mail: c.boxall@lancaster.ac.uk. Tel.: +44 1524 593109

[†]The Lloyd's Register Foundation Centre for Nuclear Engineering, Engineering Department, Lancaster University. [‡]National Nuclear Laboratory, Central Laboratory, Seascale.

ABSTRACT: Photocatalytically generated H₂O₂-driven nickel dissolution has been studied as a novel, secondary waste minimal decontamination process for nuclear process steels. Nickel corrosion experiments in dilute H₂SO₄ show that at deliberately added [H₂O₂] ≤ 1 mM, nickel dissolution occurs *via* formation and dissolution of NiOH groups; at [H₂O₂] ≥ 10 mM (pseudo-)passivation by NiO prevents this. Furthermore, Nickel also dissolves slowly in mild acid, dissolution that is significantly accelerated in the presence of photogenerated peroxide - suggesting that photocatalytically generated H₂O₂ could be used to selectively increase dissolution of Ni, and potentially steel, surfaces that normally dissolve only slowly in mild acid.

KEYWORDS: A. Nickel; B. Potentiostatic; B. Weight Loss; C. Anodic Dissolution; C. Oxidation

1. Introduction

Stainless steels are ubiquitous on nuclear sites either as construction materials or as the primary fabric of process plant components such as pipework, vessels, waste storage tanks, etc. In the case of the latter radioactive contamination, originating from the 'plate-out' of radioactive solids, colloids or metal ions onto stainless steel surfaces in plant vessels, tanks, pipes etc., is a universal problem across nuclear licensed sites. As a result, improved chemical decontamination techniques to either reduce radioactivity levels to enable man access for 'hands-on' decontamination and/or to allow for waste to be reclassified to a lower level are required.

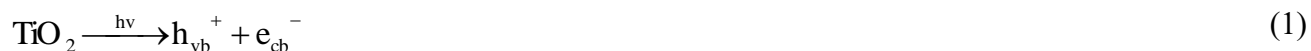
Decontamination techniques for the removal of fixed (i.e. chemically bound) contamination from metal surfaces are mostly redox chemistry based and involve either: (1) simple one step treatments such as the cerium oxidant based MEDOC process (Metal Decontamination by Oxidation with Cerium) [1-6] or high temperature citric acid wash [7], or (2) more complex multistep processes, such as the permanganate oxidant based CORD process (Chemical Oxidising Reduction Decontamination) [8-12]. Importantly, hydrogen peroxide in combination with actinide/transition metal complexants such as hydroxycarboxylic acids [2] or carbonates in the COL process (Carbonate-based Oxidative Leaching) [13-15], has proved to be a useful single step decontamination process that produces less secondary waste. However, the disadvantages of these chemical wash techniques are difficulties in accessing some parts of old plants (e.g. pipe junctions), the generation of large arisings of acidic secondary effluents (MEDOC and CORD) and often a need to use decontamination agents which are themselves incompatible with existing effluent and waste treatment processes. Therefore there is real benefit if alternative decontamination processes can be identified which offer advantages in improving access to some areas of plant and/or do not ablate non-active surfaces and/or use more benign reagents. Photocatalytic promotion of H₂O₂-based advanced oxidation processes (AOPs) may provide such an alternative decontamination option.

Photocatalysis can be loosely defined as the promotion of a reaction by the photoexcitation of a catalyst. The primary step of photocatalysis involves the absorption of light by a solid substrate

immersed in a liquid, typically aqueous, medium to create electron hole pairs which in turn generate free radicals such as OH[•] or molecular species such as H₂O₂ able to drive secondary reactions. Common applications include, *inter alia*, the driving of AOPs [16-19], precious metal recovery [20,21], and the removal of heavy elements from effluent streams [22-24]. Common photocatalysts, usually deployed in particulate form, include cadmium sulphide and the oxides of tin, tungsten and titanium, with TiO₂ the most prevalently used [25-27].

Of relevance to steel decontamination technologies is the recently reported photocatalytically driven, hydrogen peroxide mediated, dissolution of macroscopic silver surfaces by a one electron oxidation process, Ag to Ag⁺ [28]. Using a colloidal TiO₂ dispersion, hydrogen peroxide is photocatalytically generated *via* the conduction band electron driven reduction of molecular oxygen with scavenging of valence band holes provided by additional propan-2-ol in order to avoid electron/hole recombination as follows [29]:

Photocatalytic Excitation



Formation of Hydrogen Peroxide



Electron Donor (Hole Scavenger) Oxidation



In the presence of a silver surface, hydrogen peroxide undergoes a heterogeneous catalytic process decomposing to water and oxygen *via* the generation of a surface silver hydroxide [30,31]:





During the decomposition of H_2O_2 dissolution of silver occurs as a side reaction,



the extent of this reaction being small compared to the main decomposition of hydrogen peroxide.

Furthermore, this photoinduced dissolution effect is both highly controllable (switchable through application / removal of light) and spatially specific (differential dissolution rates observed from directly and partially illuminated surfaces and negligible dissolution observed from un-illuminated systems). This suggests that photocatalytically driven metal dissolution could potentially be developed into a new spatially specific, and thus secondary waste minimal, metal surface decontamination technique.

Additional advantages may accrue, especially from the potential for maximising peroxide decontamination efficiency, by photogenerating H_2O_2 *in situ* and directly adjacent to the site of contamination. As such, the severity of other components in the decontamination reagent could be reduced – including reagent acidity, a move that would be advantageous in reducing indiscriminate attack on metal surfaces during deployment (a problem with strong mineral acid-based decontamination techniques such as MEDOC) and so further reducing secondary waste arisings.

Thus, within the context of further development of photocatalytically driven metal dissolution as a decontamination technique, this paper applies this process to a more commonly encountered metal surface, nickel. While the corrosion resistance of stainless steel is pre-dominantly provided by thin iron and chromium passive oxide layers formed in response to oxidative attack, a high weight percentage of nickel is also present in 304L and 316L (low carbon) nuclear process stainless steels [32] and in steels

used in fuel cladding of UK design advanced gas cooled reactors (AGR). Addition of nickel increases oxidative resistance at neutral to alkaline pHs by widening the window of passivity and the region of immunity of stainless steels, providing improved corrosion resistance in reducing environments [33]. Nickel also increases the crystal phase stability of nuclear process steels, improving mechanical properties such as ductility, toughness and weldability [34]. As such, selective dissolution of nickel may potentially disrupt the steel surface structure through grain boundary corrosion and Ferritization, releasing adhered radionuclide contaminants.

This study is therefore novel in that it presents the first investigation of the photocatalytically-driven dissolution of a metal: (i) that is oxidised *via* a potentially slow 2 electron transfer process; (ii) that, for much of the water E_h -pH stability region, is protected against dissolution by a passivating surface layer of nickel oxide/oxyhydroxide; and (iii) is a major component of alloys that are widely used for structural and process applications – thus opening the possibility of using this technology for industrially relevant decontamination and clean-up applications. This is in contrast with the earlier work performed on silver [28], a metal that is not subject to any kinetic limitations in its one electron oxidation to form Ag^+ , does not passivate and thus is limited to predominantly ornamental uses.

While the effect of sulphuric acid on nickel dissolution [35-40] and conversely the rate of hydrogen peroxide decomposition over nickel catalysts [41-45] has been well characterised, there have been relatively few studies on the effect of deliberately added hydrogen peroxide on the rate of Ni dissolution in mild acid (pH 2 and above) solutions such as those suggested above. Schumb *et al.* report that in the presence of both high molarity hydrochloric and sulphuric acids, hydrogen peroxide is capable of dissolving metallic nickel [46]. However, in neutral and alkaline conditions, nickel shows significant resistance to hydrogen peroxide corrosion. Thus, before attempting photocatalytically driven, hydrogen peroxide mediated, dissolution of nickel, we first characterise by potentiometry and quartz crystal microgravimetry the behaviour of nickel electrodes in mildly acidic (pH 2.1 H_2SO_4) hydrogen peroxide solutions of increasing concentration *via* the electrochemical quartz crystal microbalance (QCM). As demonstrated in our previous publications [28,47], the capacity of the QCM to measure nanogram

changes in the mass of metal electrodes in real time makes it especially suitable for *in situ*, measurements of corrosion and dissolution of the type that may be expected in the nickel system studied here.

2. Experimental Section

2.1. Materials

All chemicals were of AnalaR grade or better and supplied by Sigma Aldrich (Gillingham, Dorset, UK) with the exception of 35 wt. % hydrogen peroxide supplied by Fisher Scientific Inc (Loughborough, Leicestershire, UK) and Degussa P25 Titanium Dioxide supplied by Evonik Industries (Rellinghauser Straße 1—11, Essen, Germany).

All H₂O used was doubly distilled water from a home-made still, further purified by a deionisation system (E-pure model 04642, Barnstead/Thermodyne, Dubuque, Iowa, USA) to a resistivity of $1.8 \times 10^5 \Omega\text{m}$ and a pH of 6.7.

Except where explicitly stated, all experiments were conducted in Pyrex® glassware due to its transparency to wavelengths down to 300 nm.

2.2. Quartz Crystal Microbalance Piezoelectrode Preparation

QCM piezoelectrodes comprised of polished Ni coated quartz crystals with a Cr adhesion layer (front and rear) were supplied from Testbourne Ltd. (Hassocks Wood, Basingstoke, Hampshire, UK). The crystals were AT cut quartz, with a nominal resonant frequency of 5 MHz. All crystals were solvent washed prior to use by successive washes of chloroform, acetone and finally ethanol to remove any surface contaminants.

2.3. Microgravimetric Studies of Ni Dissolution in the Presence of Deliberately Added H₂O₂

Mass changes at the QCM piezoelectrode surface, due either to material dissolution or deposition, can be taken to be directly proportional to the resultant resonant frequency change if it is assumed that the associated mass is rigidly bound to the electrode surface. This relationship is commonly expressed through the Sauerbrey equation [48]:

$$\Delta f = -C_f \Delta m \quad (9)$$

where C_f is the mass sensitivity of the 5 MHz AT-cut crystal. The value of C_f was calibrated by the electrochemical deposition and dissolution of copper *via* cyclic voltammetry [49,50] and was found to be $0.0557 \text{ Hz}^{-1} \text{ ng cm}^{-2}$, which is in excellent agreement with a theoretical value of $0.0560 \text{ Hz}^{-1} \text{ ng cm}^{-2}$.

Microgravimetric measurements of Ni dissolution in the presence of deliberately added increasing concentrations of H_2O_2 were performed in 200 mL solutions of pH 2.1 H_2SO_4 . Ni piezoelectrodes were positioned in a polytetrafluoroethylene (PTFE) holder so that only the Ni front electrode face was exposed to solution. Changes in frequency were monitored using a research quartz crystal microbalance frequency counter (Maxtek, 5980 Lakeshore Drive, Cypress, CA, USA). A detailed description of QCM theory and calibration has been described in detail previously [28].

After a one hour frequency equilibration period in solution, aliquots of H_2O_2 created from a stock solution of $10 \text{ mol dm}^{-3} \text{ H}_2\text{O}_2$ were added to achieve target test solution concentrations. All experiments were performed in the dark to avoid H_2O_2 photodecomposition and solutions were bubbled with air throughout the measurement period to facilitate solution mixing.

2.4. Study of Ni Dissolution by Photocatalytically Generated H_2O_2

The effect of photocatalytically generated H_2O_2 on the dissolution of Ni was assessed *in situ* using a combination of microgravimetry and open circuit potentiometry. QCM measurements were taken as per section 2.3. with the Ni piezoelectrode facing the lamp directly when placed within the solution reaction vessel. The solution exposed Ni layer of the Ni piezoelectrode was connected to the working electrode (WE) input of an Autolab PGSTAT10 computer controlled potentiostat (Windsor Scientific Ltd., Slough, UK) so allowing performance of simultaneous QCM and open circuit potential experiments within a conventional two electrode cell using a saturated calomel electrode (SCE, type CR5, ThermoRussell, Auchtermuchty, Fife, Scotland) as the reference. Unless otherwise stated, all potentials reported here are given versus the SCE.

H_2O_2 was photocatalytically generated using a method based on that developed by Goto *et al.* [16], where peroxide is produced by photocatalytic reduction of O_2 using TiO_2 as a photocatalyst and propan-

2-ol as a hole scavenger. Thus, a solution of 100 mL H₂SO₄ (pH 2.1), 0.53 mol dm⁻³ propan-2-ol and 0.008 g TiO₂ was prepared. Sonication was applied for 15 minutes prior to illumination in order to disperse the TiO₂ particles. Unless otherwise noted all experiments were performed under an air blanket to provide solution agitation and maximize generation of H₂O₂ *via* the photocatalytic reduction of O₂. Illumination was provided by a 30 W, UV 28 Mineralight lamp (Ultra-Violet Products Ltd, Nuffield Road, Cambridge, UK) with a peak wavelength emission at 365 nm. This wavelength was chosen in order to minimise sub-400 nm photon absorption and subsequent photodegradation of H₂O₂ while still providing a suitable UV wavelength for excitation of TiO₂.

3. Results and Discussion

3.1. Microgravimetric Studies of Ni Dissolution in the Presence of H₂O₂

In order to enable surface decontamination under less aggressive acidic conditions compared to those typically used in acidic decontamination washout techniques [1-6], studies of the photocatalytic dissolution of Ag presented in our previous publication were conducted in mild acid – specifically pH 2.1 sulphuric acid [28]. Thus, before describing the effect of deliberately added H₂O₂ on Ni surfaces it is first necessary to briefly summarise the baseline electrochemical corrosion behaviour of Ni electrodes in dilute sulphuric acid solutions.

The electrochemical behaviour of nickel electrodes in dilute sulphuric acid has been explored in detail by a number of authors [35-40]. Polarisation curves of nickel electrodes in sulphuric acid solutions have demonstrated that four different regions of behaviour can be identified. An example labelled polarisation curve of a Ni electrode in pH 2.1 H₂SO₄ is shown in Fig. 1.

Region (I) corresponds to the active dissolution region of Ni. In this region Ni metal actively dissolves into solution *via* the formation of an adsorbed surface hydroxide [37,38,40,51]:



Concurrent electrochemical quartz crystal microbalance (EQCM) experiments conducted by Itagaki *et al.* [40] and repeated in our laboratory using pH 2.1 H₂SO₄, Fig. 2, show that mass loss from a Ni piezoelectrode in this active dissolution region, also labelled as region I, is rapid.

Region (II) in Fig. 1 corresponds to the pre-passive or pseudo-passive dissolution region, this passivity arising from the formation of NiO and higher oxides at the nickel surface [38,40]. It is this pseudo-passivating behaviour of Ni that provides Ni surfaces with a level of corrosion resistance to

acidic conditions and is a feature not predicted by thermodynamic considerations of Ni electrochemical behaviour found in potential-pH diagrams [33,36,52]. As in the active dissolution region (I), Ni dissolution in region (II) proceeds *via* eqs. 9 and 10. However, during these reactions the concentration of the intermediate complex NiOH^+ increases locally to the electrode surface, until the concentration of NiOH^+ exceeds the solubility product of NiO. As a consequence, olation and oxalation reactions ensue, resulting in the precipitation of a film of NiO *via* the overall process described by eq. 12. [38,53].



This initial, very thin ($\sim 2 \text{ \AA}$ [54]), NiO film is suggested by Sato and Okamoto [37] to have a porous character, with some limited dissolution occurring from the underlying Ni surface through the oxide pores. However, further dissolution only results in maintaining and strengthening the NiO layer resulting in no net mass loss or gain, as confirmed by EQCM experiments on Ni electrodes conducted by Itagaki *et al.* and through repeat experiments in our laboratory, as seen in region II of Fig. 2 [40].

Region (III) in Fig. 1 corresponds to the region of primary passivity. Primary passivation of the surface is due to the rapid thickening of the NiO layer as the current enters steady state, increasing from 2 \AA to $\sim 2 \text{ nm}$ according to XPS studies of polarised Ni electrodes in H_2SO_4 by Hoppe and Strehblow [54]. Unlike the NiO pre-passive film, this thicker NiO film is non-porous and therefore represents a state of true passivity – as evidenced by the near absence of any mass change with increasing applied potential in region III of Fig. 2.

Region (IV) in Fig. 1 corresponds to the region of transpassive dissolution. Dissolution of Ni in this region has been suggested by Hoppe and Strehblow to occur *via* several steps. First, in the region of primary passivity and after stability of the NiO film is achieved (see above), a fine $\text{Ni}(\text{OH})_2$ overlayer of only a few monolayers is formed at the NiO-solution interface. As the potential is scanned further into the start of the transpassive region, band bending occurs within the NiO film (which is generally

accepted as a p-type semiconductor) causing the Fermi level to enter the valence band. As a consequence there is an accumulation of positive valence band holes at the NiO/Ni(OH)₂ interface, causing an oxidation of Ni(OH)₂ to NiOOH. In sulphuric acid solutions between 0.005 and 0.5 mol dm⁻³, Hoppe and Strehblow note that the so formed NiOOH film is highly soluble, dissolving to form Ni³⁺ which they detected electrochemically using a rotating ring disk electrode [54].

As summarised at the end of the introduction (section 1), there have been very few studies on the effect of H₂O₂ on Ni dissolution, especially under mild acid conditions. Thus, in order to verify the scant literature on H₂O₂-driven Ni dissolution in solutions of sulphuric acid, combined *in situ* microgravimetry/potentiometry measurements were conducted on Ni coated piezoelectrode crystals exposed to increasing concentrations of H₂O₂ from 100 μmol dm⁻³ to 1 mol dm⁻³. The results of these experiments are shown in Fig. 3 and Fig. 4 for electrode exposure times of $t \leq 60$ minutes.

Considering first the open circuit potentiometry results of Fig. 4, an increased oxidative stress is seen on the Ni piezoelectrode with increasing concentrations of H₂O₂, the measured potential reaching a rest/equilibrium value at long experiment times. For nickel electrodes immersed in 100 μmol dm⁻³ and 1 mmol dm⁻³ H₂O₂ peroxide solutions, these steady state potentials have values of +0.04 and +0.09 V vs. SCE respectively. Comparison with the polarisation curve and voltammogram of Figs. 1 and 2 respectively indicates that these values lie in the lower potential range of the pre-passive region (II) of Fig. 1, close to the region (I) / region (II) border i.e. the nickel can be considered to be slowly dissolving. In contrast, for all experiments conducted in solutions of mild sulphuric acid solutions containing concentrations of H₂O₂ of 10 mmol dm⁻³ or greater, the steady state potentials all have values greater than +0.27 V vs. SCE and so reside well within region (III) of Fig. 1 i.e. the nickel surface can be considered to be passivated.

This preliminary analysis is confirmed by the microgravimetric results of Fig. 3, which show that the addition of H₂O₂ at concentrations of 1 mmol dm⁻³ or less results in a gradual recorded mass loss over the duration of the experiments reported here i.e. the nickel is slowly dissolving in the presence of low levels of peroxide, the mechanism of which will be discussed below. Unexpectedly based on the

potential-time data of Fig. 4, the microgravimetric data of Fig. 3 indicates that the addition of H₂O₂ at concentrations of 10 mmol dm⁻³ or greater results in an initial decrease in the recorded mass that is consistent with the dissolution of the nickel surface. The size of this mass decrease gets larger with increasing concentrations of H₂O₂. Importantly, after this initial phase of dissolution, the recorded mass achieves a constant value at all concentrations of H₂O₂ and no further dissolution of the Ni surface occurs. These results can be understood as follows.

As discussed in the introduction (section 1), Baumgartner *et al.* [30] have demonstrated that the initial step in H₂O₂ driven dissolution of Ag is the formation of an adsorbed Ag hydroxide species, AgOH_{ads}, eq. 4. In light of this, it seems reasonable to propose that H₂O₂ provides a similar reaction pathway on Ni to form NiOH_{ads} as shown in eq. 13.



A consequence of the formation of NiOH_{ads} is the promotion of the dissolution of the Ni electrode surface *via* the reactions described by eqs. 10 and 11 (coupled to the reduction of H₂O₂) so resulting in the observed mass loss throughout the trace recorded at 1 mmol dm⁻³ peroxide in Fig. 3 and the initial mass losses observed in the traces recorded at peroxide concentrations of 10 mmol dm⁻³ and above in the same figure. The arresting of the initial mass loss seen at the higher peroxide concentrations in Fig. 3 may then be explained as follows.

As noted above, the open circuit potentiometry results of Fig. 4 show that the potential is driven more positive with the addition of H₂O₂. As described by Yue *et al.* [55] for the effect of deliberately added H₂O₂ on stainless steel, the observed open circuit potential is a mixed potential comprised of the anodic oxidation of Ni, eq 13a and the cathodic reduction of H₂O₂, eq. 5. The result of this is that an ever greater concentration of NiOH⁺ is generated close to the electrode surface and that, in accordance with

eq. 12, a layer of NiO is formed, retarding further dissolution from the electrode surface. Onset of the formation of this pseudo-passive nickel oxide phase can be both observed and inferred from the results of Fig. 3, where it manifests itself as a spike at $t \approx 1.5$ mins in the mass vs. time traces recorded at 10 mmol dm^{-3} , 100 mmol dm^{-3} and 1 mol dm^{-3} , respectively – the spike in the latter two traces being particularly well developed. Preceding this spike, the electrode is in its active region (region (I) of Fig. 1) and is freely dissolving. Following the apex of the spike, the mass initially increases as NiO formation competes with the underlying Ni dissolution. Immediately following the spike, the mass continues to decrease as the electrode continues to dissolve, albeit at a much reduced rate compared to rates at times preceding the spike, said dissolution being inhibited by the presence of the metal oxide layer – which itself continues to develop and consolidate. Eventually, the nickel oxide layer is robust enough to prevent underlying Ni dissolution and the electrode is passivated (region (II) of Fig. 1).

Within the context of change in frequency (Δf) vs. time data recorded during time-dependent microgravimetric measurements, differentiation of Δf with respect to time along the Δf vs. time trace yields a plot that may be considered equivalent to a representation of rate of change of electrode mass vs. time. By application of Faraday's law, this may in turn be considered to be equivalent to a plot of pseudo-dissolution or deposition current vs. time.

Such a pseudo-dissolution current vs. time plot may be readily calculated for the data of Fig. 3 (not shown). Further, a pseudo-polarisation curve for the Ni piezoelectrode under study can be produced by plotting the values of $d\Delta f/dt$ obtained at time t against the open circuit potential obtained at the same time. Pseudo-polarisation curves have been generated from Figs. 3 and 4 for those datasets that give rise to well-developed spikes in potential time traces of Fig. 3 i.e. those datasets recorded at hydrogen peroxide concentrations of 100 mmol dm^{-3} and 1 mol dm^{-3} . The resultant pseudo-polarization curves generated at these concentrations are shown in Fig. 5 as traces A and B respectively.

At a H_2O_2 concentration of 100 mmol dm^{-3} a large increase in the pseudo-current of trace A is observed at a potential of 89 mV vs. SCE. Comparison with the Ni polarisation curve of Fig. 1 and the results of Itagaki *et al.* [40] suggests that this is associated with hydrogen peroxide driven dissolution of

the Ni piezoelectrode as described above. The hydrogen peroxide in solution continues to drive the recorded potential more positive and, eventually, above an open circuit potential of 115 mV vs. SCE, the pseudo-current reduces to near 200 Hz min^{-1} as pseudo-passivation of the electrode occurs *via* the formation of NiO. This explains the arrest of the mass decrease in Fig. 3 and supports the proposed mechanism discussed above.

At a H_2O_2 concentration of 1 mol dm^{-3} the pseudo-current vs. potential trace is quite different, as shown by trace B. As for a H_2O_2 concentration of 100 mmol dm^{-3} , a large increase in the pseudo-current associated with H_2O_2 dissolution of Ni and a subsequent fall to near zero associated with surface passivation by NiO is observed. However, the transition between the regions of apparently active dissolution and pseudo-passivity occurs at $\sim 260 \text{ mV}$, a potential value that is substantially more positive than the analogous transition potential of 115 mV recorded at 100 mmol dm^{-3} . This offset of the dissolution/passivation transition to higher potentials may be attributed to the effect of hydrogen peroxide concentration on the open circuit potential ramp rate. Typically linear voltammograms and polarisation curves, such as that shown in Fig. 1, are measured at a constant scan rate/rate of change of potential with respect to time. However, the rates of change of potential with respect to time for the pseudo-polarisation curves of Fig. 5 are not constant and vary throughout the duration of the experiments represented therein. Fortunately, $\Delta E/\Delta t$ values may be readily obtained for both experimental runs of Fig. 5 by differentiating the corresponding open circuit potential vs. time plots of Fig. 3. The result of this is shown in Fig. 6.

Let us first consider the pseudo-scan rate values obtained at a H_2O_2 concentration of 100 mmol dm^{-3} , trace A of Fig. 6. At open circuit potentials $> 0.1 \text{ V}$ the scan rate is low at a value of 0.2 V min^{-1} . At open circuit potential values $< 0.1 \text{ V}$ the scan rate is substantially faster, with values up to 2.5 V min^{-1} . In comparison, at a H_2O_2 concentration of 1 mol dm^{-3} , trace B of Fig. 6, the pseudo-scan rate remains above 0.2 V min^{-1} up to open circuit potentials of $\sim 0.3 \text{ V}$. Indeed, from Fig. 4 it can be seen that upon addition of H_2O_2 to this system the imposition of an oxidative stress change of several hundred mV occurs over a period of < 1 second. Under such conditions it is likely that the change of potential is

occurring at a rate far faster than that at which the corresponding electrochemical kinetics and the kinetics of any following chemical reactions can adjust, i.e. the system kinetics cannot keep up with the rate of change of potential. Under such circumstances, the system may be said to be behaving irreversibly in an electrochemical sense. Above ~ 0.3 V, the pseudo-scan rate drops to below 0.2 V min^{-1} , the electrode/system kinetics fall into equilibrium with the open circuit potential and the system begins to behave reversibly. Thus, due to initially irreversible behaviour, the peak potential at $1 \text{ mol dm}^{-3} \text{ H}_2\text{O}_2$ is displaced to higher open circuit potentials than that seen at $100 \text{ mmol dm}^{-3} \text{ H}_2\text{O}_2$, where the pseudo-scan rate falls to lower values, and therefore reversible behaviour, at lower open circuit potentials.

To summarise, we have investigated the baseline corrosion behaviour of the infrequently studied system of nickel in mild acid peroxide solutions. We have found that at low concentrations of H_2O_2 of 1 mmol dm^{-3} or lower, dissolution of Ni occurs *via* peroxide-driven formation and oxidative dissolution of surface Ni-OH groups (i.e. the mechanism described by eqs. 13, 10 and 11) and is slow but un-inhibited by NiO passivation. At higher concentrations of H_2O_2 of 10 mmol dm^{-3} or greater, an initial period of rapid dissolution, again occurring *via* peroxide-driven formation and oxidative dissolution of surface Ni-OH groups, is followed by pseudo-passivation/passivation of the surface by NiO (eq. 12), ultimately arresting further Ni dissolution. Therefore in order for a photocatalytically induced dissolution process to proceed a H_2O_2 concentration of 1 mmol dm^{-3} or lower must be photocatalytically generated to avoid passivating the Ni electrode surface while inducing peroxide driven dissolution of Ni.

3.2. Photocatalytically Driven, H_2O_2 Mediated, Indirect Dissolution of Ni

As discussed in the introduction (section 1), one of the most widely used and effective photocatalysts for aqueous phase peroxide generation is titanium dioxide. Thus, microgravimetry and potentiometry studies of illuminated and un-illuminated Ni electrodes immersed in a suspension of colloidal TiO_2 in a solution of pH 2.1 H_2SO_4 were conducted, and results for electrode exposure times of $t \leq 900$ minutes (substantially longer than those times employed in Fig. 3 and Fig. 4) are shown in Fig. 7 and Fig. 8.

Also present in solution is propan-2-ol as a hole scavenger to promote the formation of H₂O₂ (as in the previously described Ag system [28]).

Examination of the microgravimetry results in Fig. 7 shows that in the dark and under illumination in the presence/absence of TiO₂ a large mass loss is observed after a ~300 minute period of little mass change. In order to understand these results in the context of photocatalytically driven Ni dissolution it is first necessary to discuss the electrochemical behaviour of metallic Ni in sulphuric acid in the dark, Figs. 7 and 8, Series A.

As described above, initially there is little dissolution of the Ni piezoelectrode over a period of ~300 minutes. Examination of the concurrent potential trace in Fig. 8 shows that at $t = 0$ the open circuit potential has a value of +0.141 V vs. SCE. This value can be compared with polarisation curves of a Ni piezoelectrode in pH 2 sulphuric acid produced by Itagaki *et al.* [40], as well as our own results of Fig. 1, and reveals that +0.141 V lies in the higher potential range of the pre-passive region (II) of Fig. 1, close to the region (II) / region (III) border i.e. the electrode surface is pseudo-passivated, most likely due to NiO formation as described in eq. 12. This results in little dissolution of Ni from the piezoelectrode, as observed in Fig. 7 and previously demonstrated microgravimetrically by Itagaki *et al.* and in the H₂O₂ addition results of Fig. 3. During this period of pseudo-passivity the open circuit potential gradually becomes more negative. This time dependent open circuit potential behaviour has been previously described by López-Ortiz *et al.* [56]. They report that the observed decrease in open circuit potential of a Ni electrode in response to the presence of sulphuric acid is related to a reduction in concentration of NiO at the electrode surface *via* sulphation of NiO and subsequent dissolution from the electrode *via* eq. 14:



The slow dissolution of NiO continues while the Ni electrode potential remains in the pseudo-passive region until the open circuit potential reaches a value of +0.015 V vs. SCE at ~330 minutes (again, a

substantially longer observation time than the 60 minutes employed in Fig. 3 and Fig. 4). At this value the electrode potential crosses into the active dissolution region measured by Itagaki [40] and in repeat experiments in our laboratory (region (I) of Fig. 1 and Fig. 2) and dissolution of Ni proceeds *via* eqs. 9 to 11. This results in rapid dissolution of the Ni piezoelectrode, as again demonstrated microgravimetrically by Itagaki and as observed as a rapid mass loss after ~330 minutes in the microgravimetric data of Fig. 7.

Under illumination but in the absence of TiO₂, Fig. 7 and Fig. 8 Series B, the time for the open circuit potential to drop to +0.015 V vs. SCE is slightly longer (~380 minutes) and this is reflected in the delayed onset of dissolution recorded in the concurrent microgravimetric results. This may be due to the inherent photocatalytic properties of the NiO film [57], causing a similar photocatalytic generation of H₂O₂ to that described for TiO₂, i.e. through the mechanism of eqs. 2 and 3. The result is an increased formation of NiOH_{ads} *via* the reaction mechanism in eq. 13, thus lengthening the period of pseudo-passivity, a process described in more detail below. Importantly while the time from pseudo-passivity to active dissolution is slightly increased, the rate of dissolution of the Ni piezoelectrode in the active dissolution region ($t > 380$ minutes) remains very similar to that recorded with a Ni piezoelectrode in the dark.

Under UV illumination and in the presence of TiO₂, Fig. 7 and Fig. 8 Series C, two important differences can be seen in the microgravimetric results. First, the initial period of pseudo-passivity is longer, with onset of active dissolution occurring at approximately 480 minutes. Secondly in the region of active dissolution ($t > 480$ minutes) the rate of Ni dissolution is significantly faster, with the Ni electrode completely dissolved after ~800 minutes. Calculating the peak mass loss rate in the dark and under UV illumination in the presence of TiO₂ at $t = 650$ minutes from Fig. 7 shows that in the dark the peak mass loss rate is $0.669 \mu\text{g cm}^{-2} \text{min}^{-1}$ whereas the rate of mass loss under UV illumination in the presence of TiO₂ is $3.122 \mu\text{g cm}^{-2} \text{min}^{-1}$, nearly a factor of 5 times faster.

As described in section 3.1 above, the predicted behaviour of photocatalytically generated H₂O₂ on Ni is the increased formation of NiOH_{ads} *via* the reaction mechanism in eq. 13. A consequence of the

formation of NiOH_{ads} is to promote the dissolution of the Ni electrode surface *via* the mechanism previously described in eqs. 10 and 11. However, as demonstrated previously in Fig. 4, the measured mixed potential can, upon addition of H_2O_2 at concentrations higher than 10 mmol dm^{-3} , be simultaneously driven more positive to a value where NiO layers might be expected to be formed, so suppressing electrode dissolution. Returning to Fig. 8, Series C, a small oxidative stress can be seen in the first 5 minutes of illumination (enlarged for greater clarity in the inset of that figure), taking the measured potential up to $+0.15 \text{ V vs. SCE}$. From our previous studies of photocatalytically promoted dissolution of Ag piezoelectrodes [28], this oxidative stress is due to the presence of photocatalytically generated H_2O_2 at the Ni piezoelectrode surface – which, upon comparing the measured voltage of $+0.15 \text{ V}$ with the potential-time traces of Fig. 3, we can conclude has a local concentration of between 1 to 10 mmol dm^{-3} . In analogy to the Ag system, the time dependence of both the measured voltage and piezoelectrode mass at $t < 5$ minutes in Fig. 7 and Fig. 8 are then consistent with (photocatalytically generated) H_2O_2 promoted formation of NiO at the electrode surface. Consequently, the resultant increased thickness of the oxide layer compared to that which obtains in the dark or in the absence of a photocatalyst lengthens the time taken for the NiO to undergo sulphate driven leaching *via* eq. 14. Therefore the period of pseudo-passivity is extended in comparison to experiments carried out in the dark in the presence of TiO_2 and under UV illumination in the absence of TiO_2 .

In the active dissolution region, i.e. below an open circuit potential value of 0.015 V vs. SCE at $t > 480$ minutes, the increased formation of NiOH_{ads} *via* the interaction of H_2O_2 with Ni, eq. 13, increases the rate of dissolution of NiOH^+ to Ni^{2+} *via* eqs 10 and 11. Itagaki *et al.* [40] have proposed that the rate determining step in the active dissolution of Ni to Ni^{2+} in sulphuric acid is the formation of NiOH_{ads} *via* eq. 9 and this may explain why the increase in the rate of dissolution of Ni in the presence of photocatalytically generated H_2O_2 is so drastic.

The observation of a significant increase in Ni dissolution in the presence of photocatalytically generated H_2O_2 suggests that photocatalytically generated hydrogen peroxide can be used to selectively increase the rate of dissolution of Ni surfaces that would otherwise dissolve slowly in acidic

environments – so providing a means of controlling acidic decontamination processes on Ni and potentially stainless steel *via* selective corrosion of alloyed nickel. Results also suggest that optimum rates of dissolution can be achieved by controlling the intensity of light delivered to the target metal such that the concentration of peroxide generated in the solution volume adjacent to the workpiece surface induces a mixed potential at the nickel surface that lies within the active region of Fig. 1 i.e. -0.2 to +0.1 V vs SCE. The bulk solution data of Figs. 3 and 4 suggest that this corresponds to controlling the photogenerated H₂O₂ concentration at the nickel surface in the range 1 to 10 mmol dm⁻³ – a range within which the experiment of Fig.8 already resides. This and the deployment of the technique on substrates comprised of the two other main components of stainless steels, iron and chromium, are currently the subject of further study in our laboratory.

4. Conclusion

Photocatalytic generation of hydrogen peroxide has been used to promote the active dissolution of nickel for the first time.

The process is intrinsically novel in that it is the first use of photocatalysis to drive the dissolution of a metal: (i) that is oxidised *via* a potentially slow 2 electron process; (ii) that, for much of the water E_h-pH stability region, is protected against dissolution by a passivating surface layer of nickel oxide/oxyhydroxide; and (iii) is a major component of alloys that are widely used for structural and process applications – thus opening the possibility of the use of this technology for industrially relevant decontamination and clean-up applications.

The effect on nickel piezoelectrodes of mild sulphuric acid and deliberately added H₂O₂ in mild sulphuric acid solutions has also been explored as means to understand this novel photocatalytic process. Quartz crystal microbalance experiments with nickel piezoelectrodes show that at concentrations of H₂O₂ of 1 mmol dm⁻³ or less, the dissolution of Ni occurs *via* peroxide-driven formation and oxidative dissolution of surface Ni-OH groups; the process is slow but is un-inhibited by NiO passivation. At higher concentrations of H₂O₂ of 10 mmol dm⁻³ or greater, an initial period of rapid

dissolution, again occurring *via* peroxide-driven formation and oxidative dissolution of surface Ni-OH groups, is followed by (pseudo-)passivation of the surface by NiO, ultimately arresting further Ni dissolution.

The time dependence of the open circuit corrosion behaviour of nickel electrode surfaces exposed to mild sulphuric acid, pH 2.1, in the absence of peroxide exhibits two distinct phase. The initial phase is dominated by surface passivation due to a layer of NiO which is slowly dissolved by the mild acid. This slow dissolution gradually drives the open circuit potential of the nickel in a negative direction from its passive region to its active region wherein the system enters its second phase and the nickel metal begins to dissolve.

The same two phases are also observed in the potential-time dependence of nickel electrodes in the presence of photocatalytically generated H₂O₂ produced by the UV irradiation of colloidal dispersions of TiO₂ in mild sulphuric. The initial phase is longer than that observed in the absence of photogenerated peroxide due to increased (pseudo-)passivity by NiO. Comparison of the open circuit potential measured during this period with those measured on Ni in the presence of deliberately added H₂O₂ suggests that the photocatalytically generated concentration of peroxide at the Ni surface is in the range 1 to 10 mmol dm⁻³.

However, in the second phase of active dissolution the rate of Ni dissolution is five times faster in the presence of photocatalytically generated peroxide than in its absence, with the Ni electrode completely dissolved after ~800 minutes. This suggests that photocatalytically generated hydrogen peroxide can be used to significantly and selectively increase the rate of dissolution of Ni surfaces that would otherwise dissolve slowly in acidic environments. In so doing it, provides a novel means of (i) controlling acidic decontamination processes on Ni and possibly, through selective corrosion, stainless steel and (ii) facilitates the use of milder reagents in such decontamination processes than have been used historically in e.g. the MEDOC process. Both of these factors lend themselves to the potential exploitation of this technology as a secondary waste minimal method for the removal of radioactive contamination from nuclear process steels.

These findings also suggest that optimum rates of dissolution can be achieved by controlling the intensity of light delivered to the target metal such that the concentration of peroxide generated in the solution volume adjacent to the workpiece surface induces a mixed potential at the nickel surface that lies within the active region of Fig. 1 i.e. -0.2 to +0.1 V vs SCE. Studies on solutions containing deliberately added peroxide suggest that this corresponds to controlling the photogenerated H_2O_2 concentration at the nickel surface in the range 1 to 10 mmol dm^{-3}

Acknowledgement. This work was supported by the Engineering and Physical Sciences Research Council (EPSRC), the Nuclear Decommissioning Authority (NDA) and the National Nuclear Laboratory (NNL) *via* an Industrial CASE award for RJW.

CB is supported by The Lloyd's Register Foundation. The Lloyd's Register Foundation supports the advancement of engineering-related education, and funds research and development that enhances safety of life at sea, on land and in the air.

References and Notes

- [1] J.P. Caire, F. Laurent, S. Cullie, F. Dalard, J.M. Fulconis, and H. Delagrange, AISI 304 L stainless steel decontamination by a corrosion process using cerium IV regenerated by ozone - Part I: Study of the accelerated corrosion process, *J. Appli. Electrochem.*, 33 (2003) 703-708.
- [2] J.P. Caire, S. Cullie, F. Dalard, M. Fulconis, and H. Delagrange, AISI 304 L stainless steel decontamination by a corrosion process using cerium IV regenerated by ozone - Part II: Process optimization, *J. Appli. Electrochem.*, 33 (2003) 709-715.
- [3] M. Dubourg, Hard chemical decontamination of steam-generator tube bundles, *Nucl. Eng. Des.*, 159 (1995) 123-129.
- [4] T. Suwa, N. Kuribayashi, and E. Tachikawa, Development of chemical decontamination process with sulfuric acid-cerium(IV) for decommissioning - Single step process to dissolve chromium-rich oxides, *J. Nucl. Sci. Technol.*, 23 (1986) 622-632.
- [5] T. Suwa, N. Kuribayashi, and E. Tachikawa, Development of chemical decontamination process with sulfuric acid cerium(IV) for decommissioning - System decontamination process with electrolytic regeneration of Ce-4+ from Ce-3+, *J. Nucl. Sci. Technol.*, 25 (1988) 574-585.
- [6] M. Matheswaran, S. Balaji, S.J. Chung, and I.S. Moon, Studies on cerium oxidation in catalytic ozonation process: A novel approach for organic mineralization, *Catal. Commun.*, 8 (2007) 1497-1501.
- [7] F. Di Franco, M. Santamaria, G. Massaro, and F. Di Quarto, Photoelectrochemical monitoring of rouging and de-rouging on AISI 316L, *Corros. Sci.*, 116 (2017) 74-87.

[8] D. Bradbury, Review of decontamination technology development 1977-2000, in: British Nuclear Energy Society (Ed.), Water chemistry of nuclear reactor systems 8, Vol. 1. Thomas Telford Ltd, 2001, pp. 173-178.

[9] I. Inami, Y. Sato, T. Kanasaki, N. Suzuki, A. Fujimori, A. Makihira, H. Wille, and F. Strohmer, Contribution to dose rate reduction for core internals replacement work by full system decontamination, in: British Nuclear Energy Society (Ed.), Water chemistry of nuclear reactor systems 8, Vol. 2. Thomas Telford Ltd, 2001, pp. 444-450.

[10] H. Wille and H.O. Bertholdt, The CORD UV concept for decontamination and the application experience, in: British Nuclear Energy Society (Ed.), Water chemistry of nuclear reactor systems 7, Vol. 1. Thomas Telford Ltd, 1996, pp. 317-323.

[11] H. Wille and H.O. Bertholdt, Chemical decontamination of components and systems, Nuclear Europe, 8 (1988) 41-42.

[12] H. Wille and H.O. Bertholdt, Lessons learned in full system decontamination by application of the CORD family concept, in: British Nuclear Energy Society (Ed.), Water chemistry of nuclear reactor systems 8, Vol. 1. Thomas Telford Ltd, 2001, pp. 179-184.

[13] K.W. Kim, G.I. Park, E.H. Lee, K.W. Lee, and K.C. Song, Electrolytic dissolutions of UO₂ and SIMFUEL in carbonate solutions and at several pHs, Int. J. Chem. Biol. Eng., 3 (2010) 187-190.

[14] C. Soderquist and B. Hanson, Dissolution of spent nuclear fuel in carbonate-peroxide solution, J. Nucl. Mater., 396 (2010) 159-162.

[15] M.J. Dunn, D. Bradbury, and G.R. Elder. Process for Decontamination of Radioactive Materials. Bradtec-US, Inc. Atlanta Ga. 816,467[5,322,644], 1-10. 1994. US. 3-1-1992.

- [16] H.M. Coleman, K. Chiang, and R. Amal, Effects of Ag and Pt on photocatalytic degradation of endocrine disrupting chemicals in water, *Chemical Engineering Journal*, 113 (2005) 65-72.
- [17] M.R. Hoffmann, S.T. Martin, W.Y. Choi, and D.W. Bahnemann, Environmental applications of semiconductor photocatalysis, *Chem. Rev.*, 95 (1995) 69-96.
- [18] V. Vamathevan, R. Amal, D. Beydoun, G. Low, and S. McEvoy, Silver metallisation of titania particles: effects on photoactivity for the oxidation of organics, *Chemical Engineering Journal*, 98 (2004) 127-139.
- [19] C. Hu, Y.Q. Lan, J.H. Qu, X.X. Hu, and A.M. Wang, Ag/AgBr/TiO₂ visible light photocatalyst for destruction of azodyes and bacteria, *J. Phys. Chem. B*, 110 (2006) 4066-4072.
- [20] M.I. Litter, Heterogeneous photocatalysis - Transition metal ions in photocatalytic systems, *Appl. Catal. B: Environ.*, 23 (1999) 89-114.
- [21] N.S. Foster, A.N. Lancaster, R.D. Noble, and C.A. Koval, Effect of organics on the photodeposition of copper in titanium-dioxide aqueous suspensions, *Industrial & Engineering Chemistry Research*, 34 (1995) 3865-3871.
- [22] M.I. Litter, Treatment of chromium, mercury, lead, uranium, and arsenic in water by heterogeneous photocatalysis, in: H.I. de Lasa and B. Serrano-Rosales (Eds.), *Photocatalytic Technologies*, Vol. 36. Academic Press, 2009, pp. 37-67.
- [23] C. Boxall, G. Le Gurun, R.J. Taylor, and S. Xiao, The applications of photocatalytic waste minimisation in nuclear fuel processing, in: P. Boule, D.W. Bahnemann, and P.K.J. Robertson (Eds.), *Environmental Photochemistry Part II*, Springer-Verlag Berlin, 2005, pp. 451-481.
- [24] K. Chiang, R. Amal, and T. Tran, Photocatalytic oxidation of cyanide: kinetic and mechanistic studies, *J. Mol. Catal. A: Chem*, 193 (2003) 285-297.

- [25] A. Mills and S. LeHunte, An overview of semiconductor photocatalysis, *J. Photochem. Photobiol. A: Chem*, 108 (1997) 1-35.
- [26] P. Robertson, D. Bahnemann, J.M.C. Robertson, and F. Wood, Photocatalytic detoxification of water and air, in: P. Boule, D. Bahnemann, and P. Robertson (Eds.), *Environmental Photochemistry Part II, Vol. 2* M. Springer, 2005, pp. 367-423.
- [27] T. Jafari, E. Moharreri, A.S. Amin, R. Miao, W. Song, and S.L. Suib, Photocatalytic water splitting - the untamed dream: A review of recent advances, *Molecules*, 21 (2016) 1-29.
- [28] R.J. Wilbraham, C. Boxall, and R.J. Taylor, Photocatalytically driven dissolution of macroscopic metal surfaces. Part 1: Silver, *J. Photochem. Photobiol. A: Chem*, 249 (2012) 21-28.
- [29] H. Goto, Y. Hanada, T. Ohno, and M. Matsumura, Quantitative analysis of superoxide ion and hydrogen peroxide produced from molecular oxygen on photoirradiated TiO₂ particles, *J. Catal.*, 225 (2004) 223-229.
- [30] H.J. Baumgartner, G.C. Hood, J.M. Monger, R.M. Roberts, and C.E. Sanborn, Decomposition of concentrated hydrogen peroxide on silver I. Low temperature reaction and kinetics, *J. Catal.*, 2 (1963) 405-414.
- [31] K. Goszner, D. Korner, and R. Hite, Catalytic activity of silver .1. Activity, poisoning, and regeneration during decomposition of hydrogen-peroxide, *J. Catal.*, 25 (1972) 245-253.
- [32] T.M. Hayward, I.M. Svishchev, and R.C. Makhija, Stainless steel flow reactor for supercritical water oxidation: corrosion tests, *Journal of Supercritical Fluids*, 27 (2003) 275-281.
- [33] M. Pourbaix, Nickel, in: M. Pourbaix (Ed.), *Atlas of electrochemical equilibria in aqueous solutions*, NACE International, 1974, pp. 333-334.

- [34] E.A. Avallone, T. Baumeister, and A. Sadegh, Mark's standard handbook for mechanical engineers, McGraw-Hill Professional, 2006.
- [35] L.L. Shreir, R.A. Jarman, and G.T. Burstein, Corrosion: Metal/environment reactions, Butterworth-Heinemann Ltd, 1994.
- [36] T.S. De Gromoboy and L.L. Shreir, The formation of nickel oxides during the passivation of nickel in relation to the potential/pH diagram, *Electrochim. Acta*, 11 (1966) 895-904.
- [37] N. Sato and G. Okamoto, Anodic passivation of nickel in sulfuric acid solutions, *J. Electrochem. Soc.*, 110 (1963) 605-614.
- [38] S.S. Abd El Rehim, S.M. Abd El Wahaab, and E.A. Abd El Meguid, Potentiodynamic behaviour of the nickel electrode in acid media, *Surf. Coat. Technol.*, 29 (1986) 325-333.
- [39] M. Keddam, H. Takenouti, and N. Yu, Transpassive dissolution of Ni in acidic sulfate media: A kinetic model, *J. Electrochem. Soc.*, 132 (1985) 2561-2566.
- [40] M. Itagaki, H. Nakazawa, K. Watanabe, and K. Noda, Study of dissolution mechanisms of nickel in sulfuric acid solution by electrochemical quartz crystal microbalance, *Corros. Sci.*, 39 (1997) 901-911.
- [41] G.U. Greene, The rate of decomposition of hydrogen peroxide in nickel sulfate plating baths, *J. Electrochem. Soc.*, 76 (1939) 391-400.
- [42] K. Akhtar, Decomposition of hydrogen peroxide by nickel oxide powders, *Journal of the Chemical Society of Pakistan*, 31 (2009) 59-63.
- [43] S.B. Hall, J.J. Nairn, and E.A. Khudaish, Potential and temperature dependence of hydrogen peroxide oxidation at nickel electrodes, *Phys. Chem. Chem. Phys.*, 3 (2001) 4566-4571.

- [44] G.M. Schwab and V. Mucka, Hydrogen-peroxide decomposition with nickel-oxide of various origin and influence of radiation on this process, *Zeitschrift für Physikalische Chemie-Frankfurt*, 93 (1974) 77-94.
- [45] A.B. Hart and R.A. Ross, The catalytic decomposition of hydrogen peroxide vapor by nickel oxides and promoted nickel oxides, *J. Catal.*, 2 (1963) 251-253.
- [46] W.C. Schumb, C.N. Satterfield, and R.L. Wentworth, *Hydrogen peroxide*, Reinhold Publishing Corporation, 1955.
- [47] R.J. Wilbraham and C. Boxall, The effect of acetohydroxamic acid on stainless steel corrosion in nitric acid, *Electrochemistry Communications*, 62 (2016) 52-55.
- [48] G. Sauerbrey, Verwendung von Schwingquarzen zur Wägung dünner Schichten und zur Mikrowägung, *Z. Phys.*, 155 (1959) 206-222.
- [49] C. Gabrielli, M. Keddad, and R. Torresi, Calibration of the Electrochemical Quartz Crystal Microbalance, *J. Electrochem. Soc.*, 139 (1991) 2657-2660.
- [50] G.L. Borges, K.K. Kanazawa, J.G. Gordon, K. Ashley, and J. Richer, An in-situ electrochemical quartz crystal microbalance study of the underpotential deposition of copper on Au(111) electrodes, *J. Electroanal. Chem.*, 364 (1994) 281-284.
- [51] D.V.V. Moll, R.C. Salvarezza, H.A. Videla, and A.J. Arvia, The pitting corrosion of nickel in different electrolyte solutions containing chloride ions, *J. Electrochem. Soc.*, 132 (1985) 754-760.
- [52] B. Beverskog and I. Puigdomenech, Revised pourbaix diagrams for nickel at 25-300°C, *Corros. Sci.*, 39 (1997) 969-980.

- [53] W. Paik and Z. Szklarska-Smialowska, Reflectance and ellipsometric study of anodic passive films formed on nickel in sodium hydroxide solution, *Surf. Sci.*, 96 (1980) 401-412.
- [54] H.-W. Hoppe and H.-H. Strehblow, XPS and UPS examinations of passive layers on Ni and Fe₅₃Ni alloys, *Corros. Sci.*, 31 (1990) 167-177.
- [55] Y. Yue, C. Liu, P. Shi, and M. Jiang, Passivity of stainless steel in sulphuric acid under chemical oxidation, *Corrosion Engineering, Science and Technology*, 52 (2017) 1-10.
- [56] A. López-Ortiz, V.H. Collins-Martínez, C.A. Hernández-Escobar, S.G. Flores-Gallardo, and E.A. Zaragoza-Contreras, Protection of NiO nanoparticles against leaching in acid medium by grafting of polyacrylic acid, *Mater. Chem. Phys.*, 109 (2008) 306-310.
- [57] A. Comanescu, M. Mihaly, and A. Meghea, Photocatalytic degradation of organic pollutants using NiO based materials, *U. P. B. Sci. Bull. B.*, 74 (2012) 49-60.

Figure Captions

Figure 1. Polarisation curve of a Ni piezoelectrode in pH 2.1 sulphuric acid taken at a scan rate of 0.1 V/min. Labelled regions are discussed in the text.

Figure 2. Voltamassogram of a Ni piezoelectrode in pH 2.1 sulphuric acid taken at a scan rate of 0.1 V/min. Labelled regions are discussed in the text.

Figure 3. Effect of addition of increasing H_2O_2 concentrations on the recorded mass of Ni piezoelectrodes in pH 2.1 H_2SO_4 sparged with air. (A) $100 \mu\text{mol dm}^{-3}$. (B) 1 mmol dm^{-3} . (C) 10 mmol dm^{-3} . (D) 100 mmol dm^{-3} . (E) 1 mol dm^{-3} .

Figure 4. Effect of addition of increasing H_2O_2 concentrations on the open circuit potential of Ni piezoelectrodes in pH 2.1 H_2SO_4 sparged with air. (A) $100 \mu\text{mol dm}^{-3}$. (B) 1 mmol dm^{-3} . (C) 10 mmol dm^{-3} . (D) 100 mmol dm^{-3} . (E) 1 mol dm^{-3} .

Figure 5. Pseudo-current vs. potential plot showing the effect of (A) $100 \text{ mmol dm}^{-3} \text{H}_2\text{O}_2$ and (B) $1 \text{ mol dm}^{-3} \text{H}_2\text{O}_2$, on a Ni QCM piezoelectrode in pH 2.1 H_2SO_4 sparged with air (treated with a 5 point box car average to remove experimental noise).

Figure 6. Pseudo-scan rate vs. potential plot showing the effect of (A) $100 \text{ mmol dm}^{-3} \text{H}_2\text{O}_2$ and (B) $1 \text{ mol dm}^{-3} \text{H}_2\text{O}_2$, on a Ni QCM piezoelectrode in pH 2.1 H_2SO_4 sparged with air.

Figure 7. Mass vs. time traces recorded for 15 hours of a Ni piezoelectrode in 100 mL pH 2.1 H_2SO_4 solutions of 0.53 mol dm^{-3} propan-2-ol and (A) 0.008 g TiO_2 in the dark (B) no TiO_2 and 365 nm light (C) 0.008 g TiO_2 and 365 nm light. All experiments were sparged with air throughout. For those experiments using 365 nm light, illumination was switched on at time $t = 0$ and then maintained throughout the experimental run.

Figure 8. Potential vs. time traces recorded for 15 hours of a Ni piezoelectrode in 100 mL pH 2.1 H_2SO_4 solutions of 0.53 mol dm^{-3} propan-2-ol and (A) 0.008 g TiO_2 in the dark (B) no TiO_2 and 365 nm

light (C) 0.008 g TiO₂ and 365 nm light. All experiments were sparged with air throughout. For those experiments using 365 nm light, illumination was switched on at time $t = 0$ and then maintained throughout the experimental run. Inset: Enlargement of the first 5 minutes of trace C so that the initial movement of the measured potential in the positive direction can be more clearly seen.

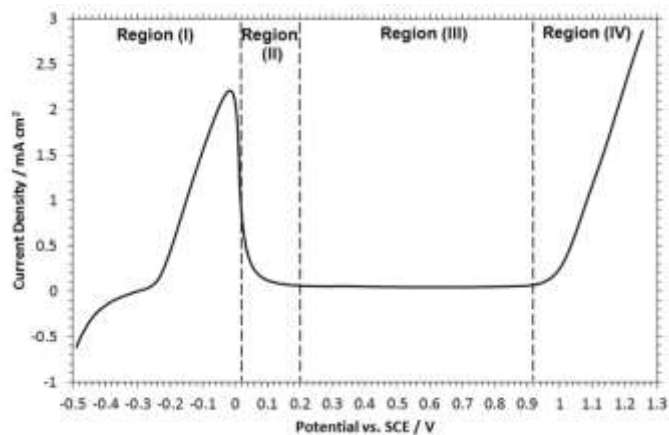


FIGURE 1

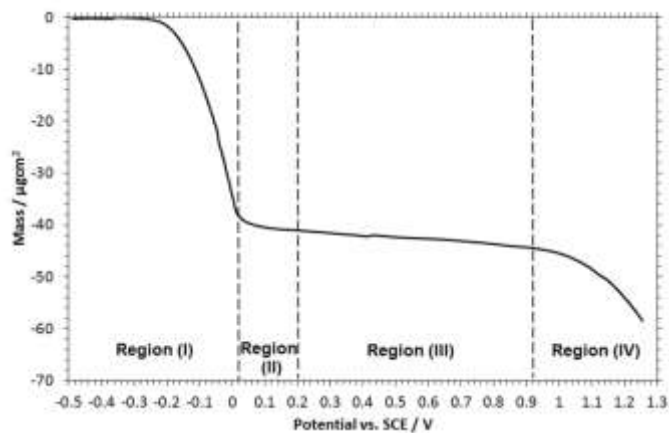


FIGURE 2

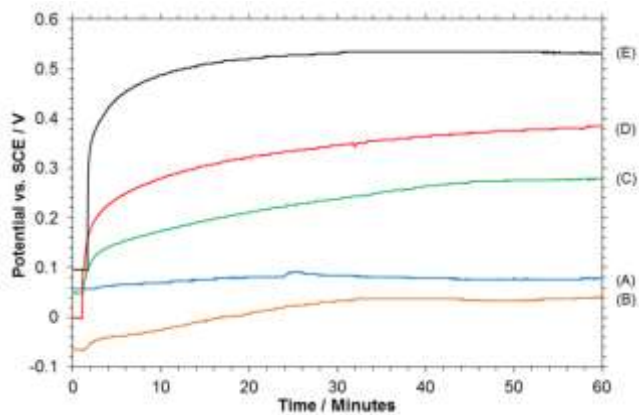


FIGURE 3

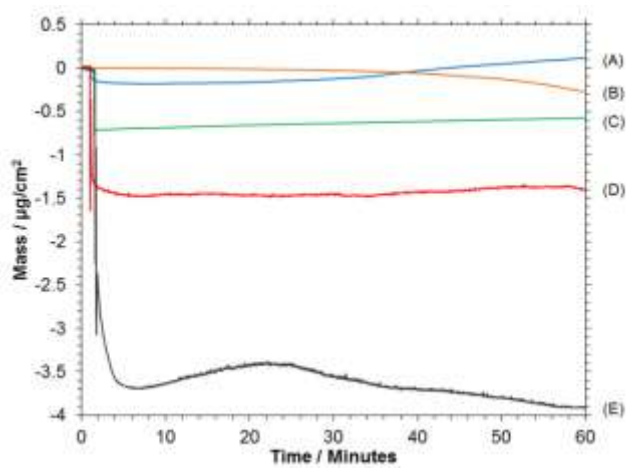


FIGURE 4

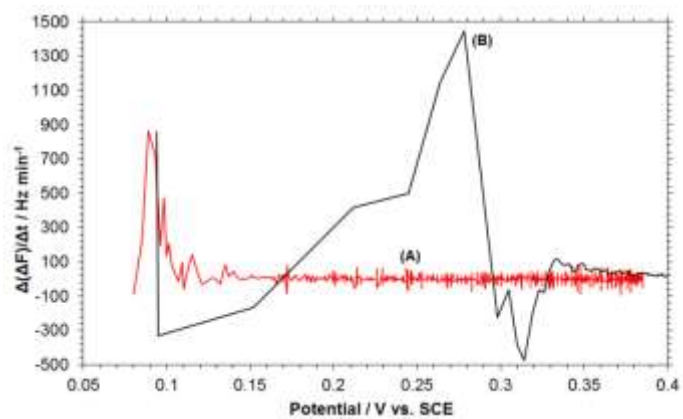


FIGURE 5

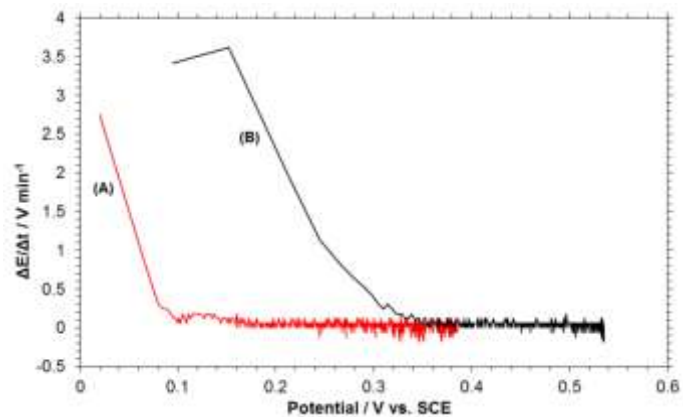


FIGURE 6

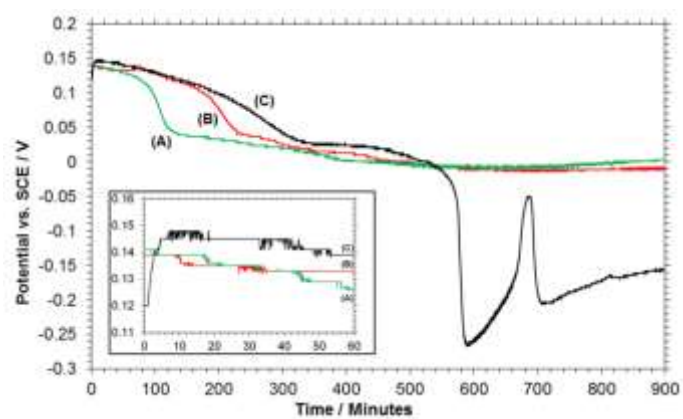


FIGURE 7

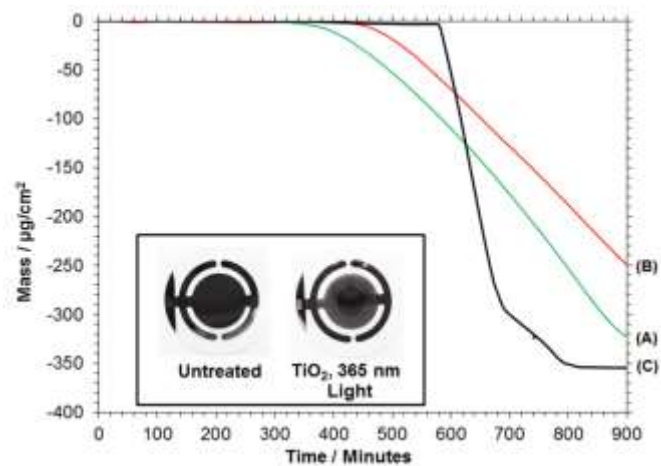


FIGURE 8